Perceptual Quality Improvement for Synthesis Imaging of Chinese Spectral Radioheliograph

Long Xu[1(✉)], Lin Ma[2], Zhuo Chen[1], Yihua Yan[1], and Jinjian Wu[3]

[1] Key Laboratory of Solar Activity, National Astronomical Observatories, Chinese Academy of Sciences, Beijing, China
lxu@nao.cas.cn
[2] Huawei Noah's Ark Lab, Hong Kong, China
[3] School of Electronic Engineering, Xidian University, Xi'an, China

Abstract. Chinese Spectral Radioheliography can generate the images of the Sun with good spatial resolutions. It employs the Aperture Synthesis principle to image the Sun with plentiful solar radio activities. However, due to the limitation of the hardware, specifically the limited number of antennas, the recorded signal is extremely sparse in practice, which results in unsatisfied solar radio image quality. In this paper, we study the image reconstruction of Chinese Spectral RadioHeliograph (CSRH) by the aid of compressed sensing (CS) technique. In our proposed method, we adopt dictionary technique to represent solar radio images sparsely. The experimental results indicate that the proposed algorithm contributes both PSNR and subjective image quality improvements of synthesis imaging of CSRH markedly.

Keywords: Compressed sensing · Solar radio astronomy · Image reconstruction · Aperture syntheis

1 Introduction

Chinese Spectral Radioheliography (CSRH) employs the aperture synthesis (AS) principle for imaging the Sun to generate the images of the Sun. AS principle synthesizes a number of small antennas to produce a larger antenna so that a better resolution can be achieved. For AS imaging system, the image resolution is determined by the maximum baseline length termed by the largest distance of two antennas rather than the diameter of a single antenna. The maximum baseline length of CSRH is 3 km, so it can achieve a good resolution determined by $r = \lambda/D$, where λ represents wavelength and D is the diameter of objective lens. AS devices record the Fourier components of observed objects instead of spatial images, where each two antennas compose of an interferometer to capture one Fourier component each time. Given n antennas, there would be $n \times (n\text{-}1)/2$ interferometers, which can record $n \times (n\text{-}1)/2$ Fourier components for each time of observation. In addition, by making use of the Earth's rotation, more Fourier components can be obtained. Nevertheless, only a small part of Fourier components are recorded, which results in blur synthesized images usually.

The synthesized images of solar radio observation can deliver the viewers the plentiful information about solar radio activities more directly and clearly. However,

Y.-S. Ho et al. (Eds.): PCM 2015, Part II, LNCS 9315, pp. 94–105, 2015.
DOI: 10.1007/978-3-319-24078-7_10

due to the extremely sparse sampling of CSRH in practice, the synthesized images usually appear to be blurring. In this paper, we study the image reconstruction of CSRH by the aid of compressed sensing (CS) technique. In the proposed method, instead of using fixed basis functions, an adaptive dictionary is learned from input images to represent solar radio images sparsely.

Studying imaging process of AS, the image degradation comes from sparse sampling of images in Fourier domain, which is formulated by the Fourier transform of a spatial image multiplied by a sampling matrix. According to Fourier theory, this degradation is equivalent to an original image convolved by a point spread function (PSF), which is characterized by a main lobe surrounded by sidelobes. Applying this PSF to images would result in blurring in images. To eliminate blurring caused by the convolution of PSF, the researchers have proposed the opposite processing, i.e., deconvolution [1–3] to recover images from their degradations. This kind of method is called "clean" algorithm. In this paper, we propose a CS-based algorithm to recover images from their sparse samplings. This method is established on the fact that image degradation of CSRH comes from sparse sampling in Fourier domain. In addition, we discuss how to meaningfully measure image quality of synthesized images of AS and how to improve subjective image quality of AS during the reconstruction process.

The remaining content of this paper is arranged as follows. Section 2 gives the introduction of synthesis imaging of CSRH. Section 3 presents the proposed image reconstruction framework for the recorded data of CSRH. Experimental results are provided in Sect. 4. Finally, the conclusion is given in Sect. 5.

2 Synthesis Imaging Principle of CSRH

As we know, the resolution of a telescope is decided by the diameter of objective lens regardless of optical or radio telescopes. Assume the wavelength of received signal λ, the telescope diameter D, the resolution is computed by

$$R = 1.22 \times \lambda / D, \tag{1}$$

which indicates the larger the diameter of a telescope, the better the resolution. Here, the resolution is given by the farthest two bright points in observed object which can be distinguished by the telescope. This is because electromagnetic waves could result in diffraction through small pinhole (such as the lens of telescope). Two electromagnetic waves with small distance would overlap after diffraction. The unit of resolution is arc of second (") which is 1/3600 deg (°). It represents the angle which is formed by two bright points in the observed object with respect to the lens of telescope. Assume the typical wave length of visible light 555 nm, (1) can be rewritten into

$$\alpha'' = 140''/D, \tag{2}$$

where the unit of D is mm, α is measured by arc of second. From (2), to get the resolution of 0.1", the diameter of objective lens would reach 1.4 m for visible light. Although α is measured by an angle, it implies the distance between two nearest points

that a telescope can distinguish. Assume the Sun is 14960 wkm far from the Earth, 0.1" represents 72.528 km in the Sun. By the same principle, there would be over 2500 m for receiving radio wave with the minimum wavelength 1 mm with the same resolution. It is impossible to build such a huge telescope in practice.

In 1950 s, the scientists proposed the aperture synthesis technique to construct an aperture synthesis telescope array consisting of a number of small telescopes. This telescope array can achieve the same resolution of a single big telescope with the diameter equaling to the largest distance between two small telescopes. This distance is named the maximum baseline length. In aperture synthesis array, the resolution is dependent on the maximum baseline length instead of the diameter of a single telescope. This technique is a breakthrough to radio wave observation, and also a milestone in the history of radio astronomy.

The aperture synthesis array employs interferometry technique to image the brightness function of the observed object. Each two antennas form an interferometer, which records Fourier coefficients instead of spatial pixel values of the observed object. Here, the two dimension Fourier space is involved, and it is also called UV space. An interferometer records one Fourier coefficient each time. Thus, an aperture synthesis array records a set of Fourier coefficients each time. In addition, it can record more Fourier coefficients by taking advantage of the earth rotation. The spatial image of an observed object is usually termed as brightness distribution/function, while its Fourier transform is named as visibility distribution/function. Assume the brightness function I (l, m), the visibility function V(u, v), I and V are Fourier transform pairs, i.e.,

$$I(l,m) = \iint V(u,v)e^{-2\pi\tau(ul+vm)}dudv. \tag{3}$$

In practice, $V(u, v)$ is not known everywhere but is sampled at particular positions on the u-v plane. The sampling can be described by a sampling function $S(u,v)$, which is zero where no data have been taken. Assume the original visibility function $V(u,v)$, the actual visibility function recorded by an AS is:

$$V^D(u,v) = V(u,v) \times S(u,v). \tag{4}$$

Applying inverse Fourier transform to (4), one can calculate the reconstructed spatial image from $V^D(u,v)$ as:

$$I^D(l,m) = \iint V(u,v)S(u,v)e^{-2\pi\tau(ul+vm)}dudv, \tag{5}$$

which is usually referred to dirty image $I^D(l,m)$ instead of the desired intensity distribution, namely clear image $I(l,m)$. According to the convolution theorem for Fourier transform, $I^D(l,m)$ is related to $I(l,m)$ by

$$I^D(l,m) = I(l,m) \otimes B^D(l,m), \tag{6}$$

where the symbol '⊗' denotes convolution, and $B^D(l,m) = \iint S(u,v)e^{-2\pi\tau(ul+vm)}dudv$ is the synthesized beam. Dirty beam or point spread function (PSF) corresponds to the sampling function $S(u,v)$.

Based on above analysis, AS has a different imaging principle from the one of a telescope with a single antenna. However, the image quality is still dependent on the PSF which terms the imaging efficiency of a general telescope. From (6), the dirty image is related with clean one by convolving a dirty beam. To recover $I(l,m)$ from $I^D(l, m)$ is an ill-posed problem. With respect to convolution operator, the straightforward method to recover $I(l,m)$ from $I^D(l,m)$ is named "deconvolution", which tries to eliminate the convolution of $B^D(l,m)$ from right side of (6). In astronomy, this kind of method is termed "Clean" algorithm, which was proposed firstly by Högbom in 1974 [1]. The clean algorithm finds the strength and position of the peak (i.e., the greatest absolute intensity) in the dirty image one-by-one, and subtracts it from the dirty image after multiplying it by the PSF. Then, an idealized "clean" beam is applied to these accumulated point sources to output a clean image. It was claimed that "clean" algorithm is good at point source which was usually taken as the model of radio sources, including solar radio source. The point radio source can be assumed to consist of pulse signals. For handling more complicated situations, such as extended source relative to point source, the variants of Högbom clean algorithm were proposed in [2] and [3].

3 Image Reconstruction for CSRH Image System

In computer science, the regularization methods with certain prior image constraints are widely used to solve ill-posed problems. The widely used prior image constraints include smoothness, local similarity, non-local similarity and sparsity. Accordingly, these corresponding regularization methods have been proposed in the literatures. In our case, we have a very sparse sampling of visibility function $V(u, v)$ in Fourier domain, so the sparse constraint is taken into consideration to formulate optimization problem, which is regarded as the decoding part of CS methods.

CS depicts a theory that an original signal can be recovered from its degradation if the signal is subject to a certain property, namely restricted isometry property (RIP) [7–9]. Assume that the degradation process of an image is depicted by:

$$\boldsymbol{y} = \boldsymbol{H}\boldsymbol{x} + \boldsymbol{n}, \tag{7}$$

where y represents the observed image, x represents the original one, H is the degradation model and n is the random noise usually assumed to be the Gaussian white noise. Since H is irreversible, it is impossible to resolve x from y by multiplying H-1 at the both sides of (7). By imposing constraints of prior image models, x can be derived from

$$\text{argmin}_x \frac{1}{2}\|\boldsymbol{H}\boldsymbol{x} - \boldsymbol{y}\|_2^2 + \lambda \cdot \Psi(\boldsymbol{x}), \tag{8}$$

where λ is the regularization parameter, Ψ(x) represents a prior image constraint, e.g., sparse constraint of natural images. Based on the sparse constraint, the researchers have

proposed corresponding regularization methods to address image denoising, super-resolution, deblur and etc. [10–12]. In our work, the sparse sampling is closely associated with the CSRH imaging system, so sparsity model is exploited in image reconstruction of CSRH imaging system.

3.1 Image Reconstruction with Sparse Constraint

Given an input vector x has N coefficients, it is sparse if there are only K ($K << N$) non-zero coefficients after a certain transform. In compressed sensing, the sparse signal needs to be further measured by the measurement matrix for compression. The perfect reconstruction can be achieved if and only if RIP is allowed [7–9]. Assume the sparse transform matrix Ψ, the sparse constraint means $\alpha = \Psi^T x$ has a small number of nonzero coefficients. Assume the measurement matrix Φ, we have the measurement on α by $y = \Phi\alpha$. Combining these two operators, we have the following equation:

$$y = \Phi\Psi^T x = \theta x, \tag{9}$$

where θ is a $N \times M$ ($M << N$) matrix, which means that the linear equation array has more unknown parameters than the number of equations. At this situation, there are some free variables, which mean that we cannot get a determined solution for this equation array. Actually, there are many solutions for this equation array. Such a problem is named an underdetermined system of equations. It is impossible to have the determined answer for an underdetermined system. So there must be other constraints for solving an underdetermined problem. Usually, we have prior models about images to be the constraints of underdetermined problem. In this work, the sparsity constraint is considered, so Eq. (8) is rewritten as

$$\text{argmin}_{\boldsymbol{x}} \frac{1}{2}\|\boldsymbol{Hx} - \boldsymbol{y}\|_2^2 + \lambda \cdot \|\boldsymbol{x}\|_0, \tag{10}$$

where $\|x\|_0$ represents l_0 norm which indicates the number of nonzero coefficients.

3.2 Sparse Representation of Image by Dictionary

It is widely accepted that natural images are sparse in Fourier, wavelet, and DCT domain. It means that natural images can be represented by a small number of coefficients after one kind of transforms mentioned above, so they can be dramatically compressed in transform domain. That's why compressed sensing was extensively exploited in image compression during the past decades. Besides compression, this prior model of natural image was exploited to establish optimization being a constraint to solve ill-posed problem, which was used to image denoising, debluring and super-resolution.

Apart from fixed basis function for representing images, the user-defined dictionary is more efficient since it is adaptive to input signal. For our concerning, the images for processing are specific instead of general. User's dictionary can be expected to be more

competitive than fixed basis functions. For establishing dictionary, there are also a plenty of methods. A general method is to cluster input image patches (blocks) into several groups. The centroids of these clusters compose the dictionary, where each centroid is named as a code word.

In this work, we employ group-based sparse representation [13, 14], which establishes dictionary over a group of patches instead of an individual patch. These patches are from both local and non-local similar patches. This group-based sparse representation processes a group of patches simultaneously in a unified framework for exploring both local and non-local similarity of natural images. An effective self-adaptive dictionary learning method for each group was designed in [13], where an adaptive dictionary D_{G_k} ($Bs \times c$) was learnt for each group x_{G_k} directly from its estimate r_{G_k} since the original image x does not exist. In practice, r_{G_k} is initialized by the observation y. Then, it is updated in each iteration by the recovered image. After obtaining r_{G_k}, we then apply SVD to it as:

$$r_{G_k} = U_{G_k} \sum G_k V_{G_k}^T = \sum_{i=1}^{m} \gamma_{r_{G_k}(i)} \left(u_{G_k(i)} v_{G_k(i)}^T\right), \tag{11}$$

where $\sum G_k$ is a diagonal matrix with the elements on its main diagonal, and $u_{G_{k(i)}}$ and $v_{G_{k(i)}}$ are the columns of U_{G_k} and V_{G_k}. Each atom in D_{G_k} for group x_{G_k} is defined as

$$d_{G_k(i)} = u_{G_k(i)} v_{G_k(i)}^T,\ i = 1, 2, \ldots, m, \tag{12}$$

where $d_{G_{k(i)}} \in R^{Bs \times c}$, so the dictionary $D_{G_k} = \left[d_{G_{k(1)}}, d_{G_{k(2)}}, \ldots, d_{G_{k(m)}}\right]$.

Each basis image, $u_i v_i$ specifies a layer of image geometry, and the sum of these layers denotes the complete image structure. The first few singular vector pairs account for the major image structure, whereas the subsequent u_i and v_i account for the finer details in an image. We illustrate this point through an example shown in Fig. 1, where the image size is 512 × 512. We can see that the first 20 pairs (z = 20) of u_i and v_i capture the major image structure, and the subsequent pairs of u_i and v_i signify the finer details in image structure. As an increasing number of u_i and v_i pairs are used, the finer image structural details appear. u_i and v_i can therefore represent the structural elements in images well.

3.3 Optimization Formulation for CSRH Imaging System

After obtaining dictionary, an image can be represented sparely by the codewords of this dictionary. In compressed sensing, this sparse representation will further undergo random measurement of the measurement matrix. In our work, a sample pattern given by the antennas configuration of CSRH [15–17] is imposed on the Fourier transform of the brightness function of the Sun (spatial image) to provide a sparse measurements of the brightness function. Relative to brightness function, the Fourier transform of brightness function is named visibility function. Given a dictionary D_G, the sparse representation of a brightness image can be written

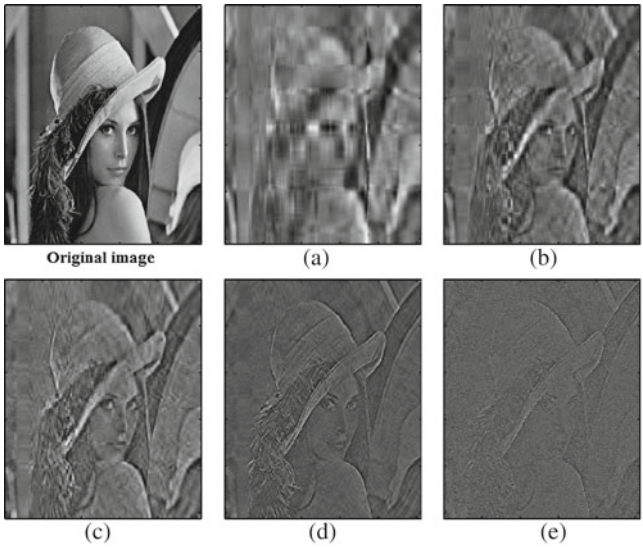

Fig. 1. The basis images ($u_i v_i$) coming from SVD (z = 10, 20, 30, 100 and 512 for (a), (b), (c), (d) and (e) respectively).

$$\boldsymbol{x} = \boldsymbol{D_G}\alpha_G, \tag{13}$$

which further undergoes the sampling of CSRH antenna configuration to have the recorded signal of visibility function as

$$\boldsymbol{y} = \boldsymbol{HD_G}\alpha_G. \tag{14}$$

Since (14) is an underdetermined problem, we have to impose sparse constraint to solve α_G from (14). With sparse constraint, we have a constrained optimization

$$\min\|\alpha_G\|_0 \, s.t. \, y = HD_G\alpha_G, \tag{15}$$

which is not convex due to l_0 norm, so it is usually to replace l_0 by l_1. Thus, the optimization formulation is finalized by

$$\hat{\alpha}_G = \text{argmin}_{\alpha_G}\|\boldsymbol{HD_G}\alpha_G - \boldsymbol{y}\|_2^2 + \lambda\|\alpha_G\|_1, \tag{16}$$

which can be solved efficiently by some recent convex optimization algorithms, such as iterative shrinkage/thresholding, split Bregman algorithms. Generally, there are three kinds of methods: greedy algorithm, convex optimization and combination of them for resolving (16).

4 Experimental Results

CSRH consists of a high frequency array (CSRH-II) with 60 antennas and a low frequency array (CSRH-I) with 40 antennas. These antennas are located in three spiral arms as shown in Fig. 2 (a) to form an AS system. For AS observation, the interferometry technique is employed to record input signal in frequency domain instead of spatial domain. Specifically, each two antennas form an interferometer which can capture one frequency component in Fourier/UV domain at each time of observation. There are 40 antennas, so we have 40 × 39/2 frequency components for one time of observation of CSRH-I. By applying inverse Fourier transform, we can obtain spatial images of observed objects.

In our simulation, we use the sample pattern of CSRH-I to generate degraded image from original ones. Here, we use the photos taken by Atmospheric Imaging Assembly (AIA) of Solar Dynamics Observatory (SDO) [18]. The sample pattern of CSRH-I is shown in Fig. 2(b), which is named UV coverage, and represented by a matrix in UV domain or frequency domain. The corresponding spatial form of Fig. 2(b) is called PSF or "dirty beam" which is the inverse Fourier transform of UV coverage. It can be

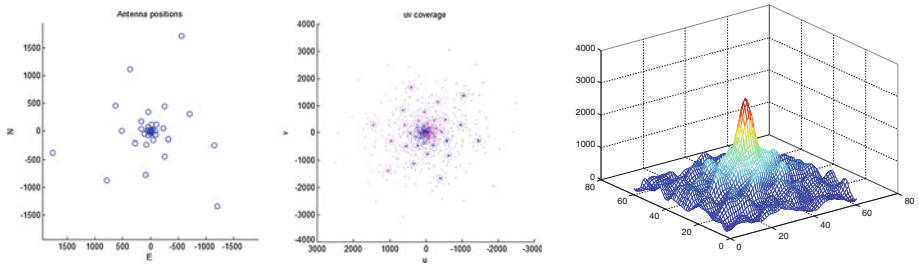

(a) Antennas configuration (b) UV coverage (c) Point spread function

Fig. 2. Aperture synthesis of CSRH-I. (a) Antennas configuration (b) UV coverage (c) Point spread function.

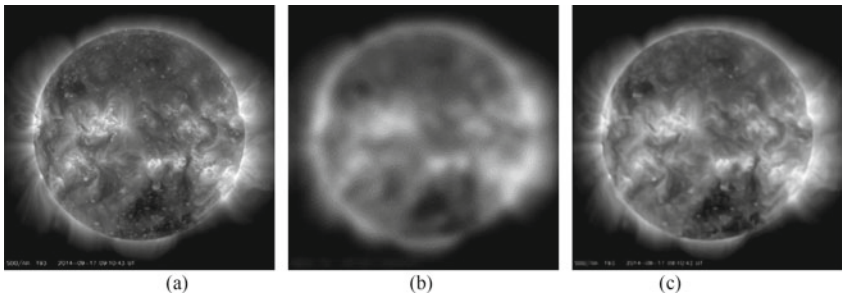

(a) (b) (c)

Fig. 3. Image reconstruction of CSRH. (a) An image recorded by SDO/AIA at 193; (b) The imaging result of CSRH ((a) is convolved by the PSF show in Fig. 2 (c)); (c) The recovered image from (b) by using the proposed algorithm.

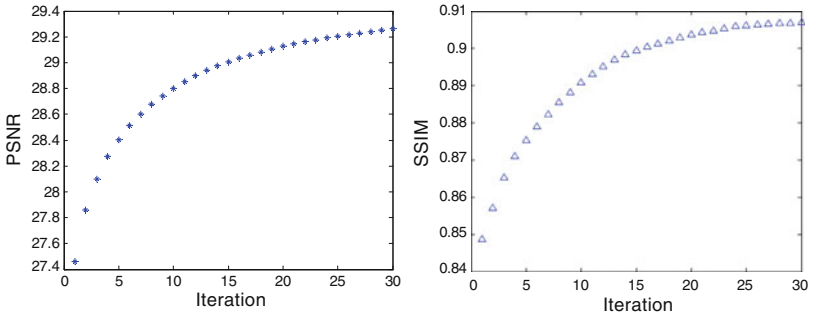

Fig. 4. PSNR/SSIM of reconstructed image over iteration.

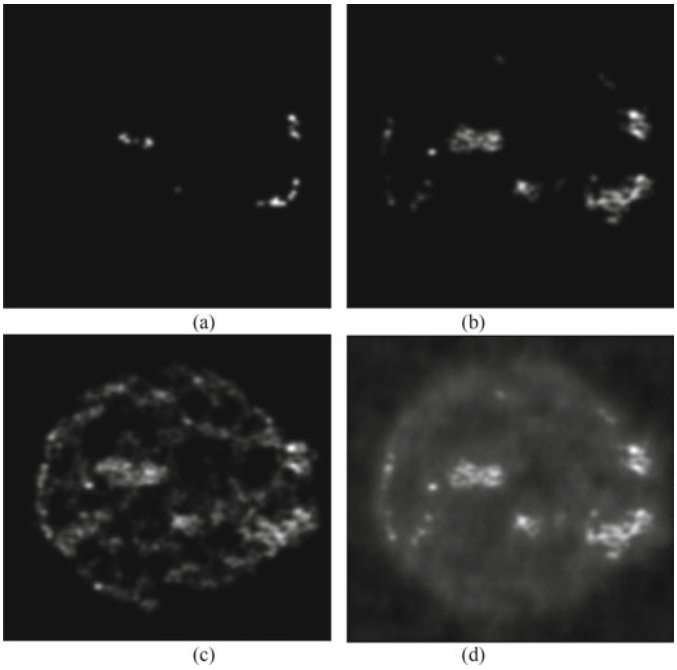

Fig. 5. The reconstructed image by using Högbom clean algorithm ((d) is the reconstructed image with 400 iterations; (a)-(c) only show the peaks without solar disk background (a) 40 iterations; (b) 400 iterations; (c) 4000 iterations).

observed that CSRH-I has a very sparse UV coverage, so only a small part of Fourier components can be recorded by CSRH-I. It is impossible to have a spatial image as clear as the original one. Fortunately, the low frequency components (center part of UV coverage) are with dense sampling. The low frequency is regarded to have more important geometry information of an image.

Simulating the process of AS imaging system, an original image is given in Fig. 3 (a). However, we can only obtain its degraded one shown in Fig. 3(b) by CSRH-I system. This process can be represented that an image is convolved by a dirty beam, e.g., Fig. 2(c). As shown in Fig. 2(c), there are a certain amount of sidelobes apart from main lobe in a PSF, so an original image would be blurred by convolving such a PSF. To improve image quality regarding such a convolution process, "clean" algorithms [1–6] have been proposed to fulfill corresponding deconvolution process, i.e., eliminate convolution effect of the PSF on the original image. These "clean" algorithms are straightforward, and therefore behave more applicable and robust. Associating sparse sampling process of an AS system, CS-based [19–23] algorithms have been explored to recover images from degraded ones. The captured signals were regarded to be sparse with respect to Fourier or wavelet basis in these algorithms.

In this work, we explore user-defined dictionary for more efficient sparse representation of image. This dictionary based CS algorithm is adaptive to input signal, and therefore could acquire better efficiency. The proposed algorithm for CSRH imaging is formulated in (16). To solve (16), the Split Bregman Iteration (SBI) is employed. It concerns a series of interactions. In each round of iteration, the reconstructed image is improved with respect to image quality. The iteration is terminated after 30 iterations or beyond a given threshold which is given by the PSNR difference between two successive iterations. We give an example of the iteration in Fig. 4 to illustrate the procedure of iteration. It can be observed the image quality of reconstructed image is improved step by step. From Fig. 4, the improvement of image quality is significant. There is 5 dB PSNR gain of the final reconstructed image over the worst one. For better measuring subjective image quality, we also employed SSIM [24] to evaluate image quality. The SSIM is regarded to be better for representing image structures. The SSIM for each iteration is also shown in Fig. 4. The final reconstructed image is shown in Fig. 3(c), it can be obviously observed that the better subjective image quality is obtained. Comparing with Fig. 3(b), the reconstructed image presents clear edges and structures can be identified in Fig. 3(c).

For comparing with the state-of-the-art algorithms, we implement Högbom clean algorithm on the blurred image of CSRH. The experimental results are shown in Fig. 5. From Fig. 5, we can observe that more and more peaks which represent point sources in the blurred image are identified with the increase of iterations. In theory, all these point sources can be figured out. Then, convolving these point sources with an idea beam instead of the dirty beam, one can obtain a cleaned image. However, these point sources interfere with each other if these point source are closely related. That's why the results of Högbom clean algorithm is not as satisfied as that it claimed in our simulation.

5 Conclusion

This paper presented a CS-based image reconstruction algorithm for CSRH imaging system. By using user-defined dictionary, the images of CSRH can be better represented sparsely. The better image quality can be obtained by the proposed CS-based image reconstruction algorithm. Comparing with clean algorithms, the proposed

algorithm can better recover the high frequency components which represent fine image geometry.

Acknowledgment. This work was partially supported by a grant from the National Natural Science Foundation of China under Grant 61202242, 100-Talents Program of Chinese Academy of Sciences (No. Y434061V01).

References

1. Hőgbom, J.A.: Aperture synthesis with a non-regular distribution of interferometer baselines. Astron. Astrophys. Suppl. **15**, 417 (1974)
2. Thompson, A.R., Moran, J.M., Swenson, G.W., Wakker, B.P., Schwarz, U.J.: The Multi-Resolution CLEAN and its application to the short-spacing problem in interferometry. Astron. Astrophys. **200**, 312–322 (1988)
3. Cornwell, T.J.: Multi-Scale Clean Deconvolution of Radio Synthesis Images. arXiv: 0806.2228
4. Weir, N.: A multi-channel method of maximum entropy image restoration. In: ASP Conference Series 25: Astronomical Data Analysis Software and Systems I, p. 186 (1992)
5. Cornwell, T.J., Evans, K.F.: A simple maximum entropy deconvolution algorithm. Astron. Astrophys. **143**, 77–83 (1985)
6. Starck, J.L., Pantin, E., Murtagh, F.: Deconvolution in astronomy: a review. Publ. Astr. Soc. Pacific **114**, 1051–1069 (2002)
7. Cand`es, E., Romberg, J., Tao, T.: Robust uncertainty principles: exact signal reconstruction from highly incomplete frequency information. IEEE Trans. Inform. Theory **52**, 489–509 (2006)
8. Donoho, D.L.: Compressed sensing. IEEE Trans. Inf. Theory **52**(4), 1289–1306 (2006)
9. Donoho, D.L., Huo, X.: Uncertainty principles and ideal atomic decompositions. IEEE Trans. Inform. Theory **47**, 2845–2862 (2011)
10. Elad, M., Aharon, M.: Image denoising via sparse and redundant representations over learned dictionaries. IEEE Trans. Image Process. **15**(12), 3736–3745 (2006)
11. Buades, A., Coll, B., Morel, J.M.: A review of image denoising algorithms, with a new one. Multiscale Model. Simul. **4**(2), 490–530 (2005)
12. Yang, J., Wright, J., Huang, T.S., et al.: Image super-resolution via sparse representation. IEEE Trans. Image Process. **19**(11), 2861–2873 (2010)
13. Zhang, J., Zhao, D.B., Gao, W.: Group-based sparse representation for image restoration. IEEE Trans. Image Process. (TIP) **23**(8), 3336–3351 (2014)
14. Zhang, J., Zhao, D.B., Xiong, R.Q., Ma, S.W., Gao, W.: Image restoration using joint statistical modeling in a space-transform domain. IEEE Trans. Circuits Syst. Video Technol. (TCSVT) **24**(6), 915–928 (2014)
15. Yan, Y., Wang, W., Liu,F., Geng, L., Zhang, J.: Radio imaging-spectroscopy observation of the sun in decimeteric and centimetric wavelengths. In: Solar and Astrophysical Dynamos and Magnetic Activity, Proceeding of IAU Symposium, no. 294, pp. 489–494 (2012)
16. Yan, Y., Zhang, J., Wang, W., Liu, F., Chen, Z., Ji, G.: The Chinese spectral Radioheliograph-CSRH. Earth Moon Planet. **104**, 97–100 (2009)
17. Du, J., Yan, Y.H., Wang, W.: A simulation of imaging capabilities for the Chinese Spectral Radioheliograph. In: IAU Symposium, pp. 501–502 (2013)
18. http://sdo.gsfc.nasa.gov/

19. Li, F., Cornwell, T., de Hoog, F.: The application of compressive sampling to radio astronomy I: deconvolution. Astron. Astrophys. **528**(A31), 1–10 (2011)
20. Li, F., Brown, S., Cornwell, T., de Hoog, F.: The application of compressive sampling to radio astronomy II: faraday rotation measure synthesis. Accepted Astron. Astrophys. **531**, A126 (2011)
21. Wenger, S., Magnor, M., Pihlström, Y., et al.: SparseRI: A compressed sensing framework for aperture synthesis imaging in radio astronomy. Publ. Astron. Soc. Pac. **122**(897), 1367–1374 (2010)
22. Bobin, J., Starck, J.L., Ottensamer, R.: Compressed sensing in astronomy. IEEE J. Sel. Top. Sign. Process. **2**(5), 718–726 (2008)
23. Wiaux, Y., Jacques, L., Puy, G., et al.: Compressed sensing imaging techniques for radio interferometry. Mon. Not. Roy. Astron. Soc. **395**(3), 1733–1742 (2009)
24. Wang, Z., Bovik, A.C., Sheikh, H.R., Simoncelli, E.P.: Image quality assessment: from error visibility to structural similarity. IEEE Trans. Image Process. **13**(4), 600–612 (2004)